Bioisosteric discovery of NPA101.3, a second generation RET/VEGFR2 inhibitor optimized for single-agent polypharmacology

Marialuisa Moccia,[1,†] Brendan Frett,[2,6,†] Lingtain Zhang,[2] Rajiv Lakkaniga,[2] David C. Briggs,[3] Rakhee Chauhan,[3] Annalisa Brescia,[1] Giorgia Federico,[1] Massimo Santoro,[1] Neil Q. McDonald,[3,4] Hong-yu Li,[2,6*] and Francesca Carlomagno[1,5*]

†Marialuisa Moccia and Brendan Frett contributed equally to this work.

[1]Dipartimento di Medicina Molecolare e Biotecnologie Mediche, Università di Napoli "Federico II", 80131, Napoli, Italia; [2]Department of Pharmaceutical Sciences, College of Pharmacy, University of Arkansas for Medical Sciences, Little Rock, AR 72205, USA; [3]Signalling and Structural Biology Laboratory, The Francis Crick Institute, London, NW1 1AT UK; [4]Institute of Structural and Molecular Biology, Department of Biological Sciences, Birkbeck College, London, WC1E 7HX, UK; [5]Istituto di Endocrinologia ed Oncologia Sperimentale del CNR, 80131, Napoli, Italia; [6]Synactix Pharmaceuticals, Inc., Tucson, AZ 85718, USA.

***Corresponding Authors:** Hong-yu Li, Department of Pharmaceutical Sciences, College of Pharmacy, University of Arkansas for Medical Sciences, Little Rock, AR 72205, United States; (Ph. 5012961154; HLi2@uams.edu); Francesca Carlomagno, Dipartimento di Medicina Molecolare e Biotecnologie Mediche, Università di Napoli "Federico II" via S. Pansini 5, 80131 Napoli-Italy (Ph. +390815455561; Fax: +390817462685; francesca.carlomagno@unina.it)

Keywords: kinase; tyrosine kinase inhibitor; targeted therapy; thyroid cancer; lung adenocarcinoma

Financial support: This study was supported by NIH 1R01CA197178-01A1R grant (to HL). In addition, HL was supported by NIH 1R01CA194094-010 and UAMS start-up funding; FC was supported by the Associazione Italiana per la Ricerca sul Cancro (AIRC); NQM was supported by the Francis Crick Institute, which receives its core funding from Cancer Research UK (FC001115), the UK Medical Research Council (FC001115) and the Wellcome Trust (FC001115). RC was supported by a grant to NQM from the Association for Multiple Endocrine Neoplasia Disorders MTC Research Fund. This work was also supported by an Institutional Development Award (IDeA) from the National Institute of General Medical Sciences of the National Institutes of Health under grant number "P20 GM109005", by the UAMS Seeds of Science cancer research grant and by a grant from the American Thyroid Association (ATA/Thyca) and by the POR Campania FESR 2014-2020 "SATIN" grant

Disclosure of Potential Conflicts of Interest: B. Frett and H.Y. Li have ownership interest in Synactix Pharmaceuticals, Inc. F. Carlomagno, B. Frett, M. Santoro, and H.Y. Li are inventors of patent WO/2015/187818. D.C. Briggs, R. Chauhan and N.Q. McDonald declare no potential conflicts of interest.

ABSTRACT

RET receptor tyrosine kinase (RTK) is a driver oncogene in human cancer. We recently identified the clinical drug candidate Pz-1, which targets RET and VEGFR2. A key *in vivo* metabolite of Pz-1 is its less active demethylated pyrazole analogue. Using bioisosteric substitution methods, here, we report the identification of NPA101.3, lacking the structural liability for demethylation. NPA101.3 showed selective inhibitory profile and an inhibitory concentration 50 (IC_{50}) of <0.001 μM for both RET and VEGFR2. NPA101.3 inhibited phosphorylation of all tested RET oncoproteins as well as VEGFR2 and proliferation of cells transformed by RET. Oral administration of NPA101.3 (10 mg/kg/day) completely prevented formation of tumours induced by RET/C634Y-transformed cells, while it decreased, but did not abrogate, formation of tumours induced by a control oncogene (HRAS/G12V). The balanced synchronous inhibition of both RET and VEGFR2, as well the resistance to demethylation, renders NPA101.3 a potential clinical candidate for RET-driven cancers.

INTRODUCTION

RET (REarranged during Transfection) is the receptor tyrosine kinase (RTK) for neurotrophic factors of the GDNF (glial cell line-derived neurotrophic factor) family (1). In several human cancers, RET rearrangements lead to the formation of chimeric oncoproteins, containing the RET tyrosine-kinase (TK) domain fused to the N-terminal region of heterologous proteins. These include: papillary thyroid carcinoma (PTC) (2), medullary thyroid carcinoma (MTC) (3), lung adenocarcinoma (4-6), chronic myeloproliferative disorders (7, 8), Spitz melanoma (9), colon (10, 11), breast (12) and salivary duct (13) carcinomas. CCDC6-RET rearrangement has also been found in EGFR mutant lung adenocarcinoma patients who had progressed upon EGFR TKI treatment (14). In addition, various types of germline point mutations activating the RET kinase are the causative event of hereditary MTC, in the frame of multiple endocrine neoplasia type 2 (MEN2A, MEN2B) syndromes. Somatic RET mutations, mostly RET/M918T, are commonly associated (around 50% of cases) to sporadic MTC (1, 15). Finally, RET is overexpressed in several malignancies including breast (16, 17) and pancreatic (18, 19) carcinoma.

RET targeting with tyrosine kinase inhibitors (TKIs) has emerged as a promising molecular approach for the treatment of cancer (20, 21). Two TKIs, Vandetanib and Cabozantinib, were found to exhibit VEGFR2 and RET activity (22, 23). These two drugs have been approved to treat MTC because of their capability to prolong progression-free survival (24, 25). In addition, Sorafenib and Lenvatinib, two multikinase inhibitors with activity against RET, have been approved for the treatment of radioiodine-refractory differentiated thyroid cancer (26, 27). Novel TKIs, BLU-667, LOXO-292 and RXDX-105, have recently demonstrated promising clinical activity in RET-driven cancers (28-30).

Toxicity, due to on- or off-targets effects, and resistance formation may limit efficacy of TKIs in clinical practice. We sought out to set up a fragment-based chemical screen to

identify novel RET inhibitors. This approach lead to the clinical candidate Pz-1, a type-2 TKI directed against RET and VEGFR2 (31).

In vivo stability is a critical factor that directly determines efficacy (32). Through completion of investigative new drug (IND) studies, a demethylated less active metabolite of Pz-1 was identified. Here, by applying bioisosteric substitution of the Pz-1 site susceptible to demethylation, we report the identification of NPA101.3, as a novel clinical TKI candidate and its characterization through *in vitro* and *in vivo* assays.

RESULTS

Discovery of NPA101.3. During IND-studies of Pz-1, a series of *in vivo* metabolites were identified; via Phase 1 metabolic systems, Pz-1 is oxidized, hydrolysed, or demethylated generating a less active derivative (Fig. 1 and data not shown). Hydrolysis and initial oxidation occur at the selectivity region, which is the region of Pz-1 that enters the allosteric pocket of both RET and VEGFR2. Any modification to reduce metabolism at this region can alter selectivity and inhibitory profiles and, therefore is likely to alter the optimized RET/VEGFR2 inhibitory profile. Another major, metabolic pathway of Pz-1 is initiated via the Phase 1 demethylation of methylpyrazole to generate Pz-1a. In turn, Pz-1a is further biotransformed via oxidation (to Pz-1b) or oxidation and sugar conjugation through Phase 2 systems (to Pz-1c). Interestingly, the methylpyrazole substituent of Pz-1 is oriented towards the solvent and is not expected to contribute significantly to selectivity profiles (31, 32) (Fig. 1).

Bioisosteric replacement of the methylpyrazole of Pz-1 was investigated to generate an alternative clinical candidate with similar polypharmacological profile but resistance to demethylation. In both RET and VEGFR2, the methylpyrazole binds to solvent exposed regions, which can accommodate a variety of substituents. SAR studies have shown that replacement of methylpyrazole with various five-member ring systems decreases inhibitory activity (31). Therefore, substitution with polar, electron-deficient (methylsulfonyl)benzene was investigated. The methylsulfonyl group occupies the same chemical space as the methyl pyrazole and has the same hydrogen binding pattern at the computer modelling (data not shown); therefore, it is expected not to affect the pharmacological activity of the drug as compared to methylpyrazole. Importantly, analogues containing (methylsulfonyl)benzene do not carry the structural liability of demethylation. Therefore, the (methylsulfonyl)benzene was chosen as an appropriate bioisosteric replacement for methylpyrazole, to obtain the novel

compound designated NPA101.3 (Fig. 1). The chemical synthesis of NPA101.3 is described in the Supplementary information.

Computational modelling of NPA101.3. NPA101.3 was modelled in the RET kinase DFG (aspartic acid [D892], phenylalanine [F893], glycine [G894])-out computational model as previously described (Fig. 2) (31). The model suggested that NPA101.3 binds to RET kinase in its inactive (DFG-out) conformation, as it is characteristic of type-2 TKIs (33). The benzimidazole moiety acts as the 'warhead', making a key hydrogen bond with A807 at the RET ATP binding site (hinge-region). The benzimidazole also forms two π-π stacking interactions with Y806. The *p*-sulfone substituent displays orientation towards the solvent and engages K728 through a cation-π interaction. The amide region interacts with D892 from the DFG motif through a hydrogen bond. This interaction opens-up a novel lipophilic pocket, which is effectively filled by *tert*-butyl isoxazole. The modelling predicted NPA101.3 to bind RET with high affinity and with a projected ΔG of -11.4 k/cal mol. Moreover, the model indicated that binding of NPA101.3 was not influenced by substitutions of V804, which is the gatekeeper residue whose replacement with a methionine or a leucine confers resistance to Vandetanib, Cabozantinib, and several other inhibitors (Fig. 2) (29, 34-36). NPA101.3 was also predicted to bind VEGFR2 with comparable high affinity (Fig. 2). Indeed, similar to Pz-1, the free rotation of the methylene linker permits tailored orientation of the isoxazole in the allosteric pocket of both RET and VEGFR2 enabling balanced inhibition of both kinases (31).

Kinase inhibitory activity of NPA101.3. We tested the ability of NPA101.3 to inhibit RET, the RET/V804M mutant, and VEGFR2 in an *in vitro* kinase assay. To determine if NPA101.3 tightly bound the kinase, we used high concentration of ATP (190 μM). Such a high concentration is orders of magnitude greater than the Km for either RET or VEGFR2 and

reflects the high intracellular concentration of ATP (1-10 mM). NPA101.3 exhibited an inhibitory concentration 50 (IC_{50}) of 0.001 μM for RET, 0.008 μM for RET/V804M, and 0.003 μM for VEGFR2. Thus, NPA101.3 represents a novel RET/VEGFR2 dual inhibitor with a pharmacological profile similar to Pz-1.

To further investigate NPA101.3 binding to RET, a thermal shift assay was performed to monitor protein melting temperature. This assay determines the drug-induced increase in the melting temperature (ΔTm) of the isolated RET kinase domain, which reflects the stability of the kinase-ligand complex (37, 38) and correlates with the inhibitor IC_{50} (39). Addition of NPA101.3 increased the thermal stability of active and phosphorylated RET by a dramatic ΔTm of 16 °C ± 1.1 °C, over a time course of 240 minutes (Fig. 3C; a representative experiment is reported in Fig. 3A). This was consistent with values seen for type-2 inhibitors, such as Sorafenib, stabilising a DFG-out inactive conformer (40). We observed the same magnitude of thermal shift by NPA101.3 for wild type and V804M (Fig. 3B), confirming that the compound is insensitive to gatekeeper mutation. In contrast, a substantially smaller ΔTm shift of 6.1°C ± 3.3 °C was observed with the type-1 compound PP1 (Fig. 3C), consistent with our previous published data (38). As expected, the type-1 inhibitor PP1 was sensitive to gatekeeper mutation (Fig. 3C). We conclude that NPA101.3 binds tightly to both wild type and V804M RET kinase domain in a type-2 binding mode.

Finally, NPA101.3, at a concentration of 100 nM, was subjected to a kinome scan against a 96 kinases panel representing major kinome clusters (Supplementary Information, Table S1). The compound featured good selectivity, displaying strong binding activity (>90% bound) for only 7 additional kinases (CSF1R, FRK, HCK, LYN, MKNK2, TRKA, and TRKC) and weak binding (>10-35% bound) for another 6 kinases (Supplementary information Table S1 and Fig. S1). It is important to note that measurement of binding affinity,

that is based on control-ligand displacement (Kd), is more sensitive than the *in vitro* kinase assay. In conclusion, NPA101.3 represents a highly selective type-2 kinase inhibitor.

NPA101.3-mediated inhibition of RET and VEGFR2 phosphorylation and signalling. Fibroblasts transfected with RET/C634R were treated with increasing doses of NPA101.3, ranging from 0.1 to 10.0 nM. RET autophosphorylation was assessed by Western blotting using two different antibodies able to recognize phosphorylated Y905, located in the RET kinase activation loop, or Y1062, a multidocking site involved in RET downstream signalling (41). As shown in Figure 4A, RET phosphorylation started to be inhibited at 0.3 nM and was almost completely blocked at 3.0 nM. NPA101.3 also inhibited other MTC-associated RET oncogenic point mutants, including RET/M918T, RET/A883F, and RET/V804L/M (Fig. 4B). Rearranged RET oncoproteins (CCDC6-RET, NCOA4-RET, FGFR1OP-RET) were highly sensitive to NPA101.3 inhibition, as well (Fig. 4C). Finally, 1.0 nM NPA101.3 reduced ligand-induced VEGFR2 autophosphorylation; inhibition was virtually total at 10.0 nM, indicating that NPA101.3 has similar inhibitory activity for VEGFR2 and RET (Fig. 4D).

NPA101.3 inhibited RET autophosphorylation and signalling along the SHC/MAPK pathway in human cancer cell lines endogenously expressing RET oncogenic variants, including MTC cell lines, TT (RET/C634W) and MZ-CRC-1 (RET/M918T), PTC cell line TPC-1 (CCDC6-RET); in the lung adenocarcinoma cell line Lc-2/ad (CCDC6-RET) only RET and SHC (but not MAPK) de-phosphorylation was detectable (Supplementary information, Fig. S2). Virtually no effect on SHC/MAPK signalling was identified in control cell lines lacking RET oncogenes, including Nthy-ori-3.1 thyroid follicular cells, BCPAP and 8505-C, derived from thyroid cancers negative for RET oncogenes, and PC-9, A549 and CALU-1, derived from lung adenocarcinomas negative for RET oncogenes (Supplementary information, Fig. S3).

NPA101.3-mediated inhibition of RET-driven cell proliferation. The murine pro–B cell line Ba/F3 requires IL-3 for proliferation and survival; this dependency is bypassed by active tyrosine kinases. Therefore, the Ba/F3 cell line is a standard cell culture model to determine activity and drug-mediated inhibition of tyrosine kinases (42). Accordingly, stable transfection of RET/C634R, RET/M918T and CCDC6-RET oncoproteins promotes IL-3-independent growth (Fig. 5). Treatment with NPA101.3 blunted RET-driven (IC_{50} of 1.6-3.1 nM), but not IL-3-driven parental Ba/F3 cell proliferation (Fig. 5), parallel to inhibition of RET phosphorylation (Supplementary information Fig. S4).

NPA101.3 inhibited proliferation of RET mutant TT, MZ-CRC-1, TPC-1 and Lc-2/ad human cancer cells with an IC_{50} of 0.67-3.6 nM (Supplementary information, Fig. S5 and Table S2). The IC_{50} dose for all human RET-negative cells was greater than 100.0 nM, confirming compound selectivity (Supplementary information, Fig. S6 and Table S2).

NPA101.3 inhibits tumorigenicity of RET-transformed cells. The IC_{50} dose for NPA101.3-mediated NIH3T3 RET/C634Y cell proliferation inhibition was 4.17 nM; virtually no effect was observed on proliferation of NIH3T3 HRAS/G12V cells up to 100.0 nM (Supplementary information Fig. S7). At 10.0 nM, the compound almost completely inhibited phosphorylation of RET and SHC, and attenuated phosphorylation of MAPK, in NIH3T3 RET/C634Y cells, while virtually no effect was detectable in NIH3T3 HRAS/G12V cells up to a dose of 100.0 nM (Supplementary information Fig. S8).

In vivo target (RET and VEGFR2) inhibition was studied by treating animals grafted with NIH3T3 RET/C634Y cells at different doses (0.3, 1 or 3 mg/kg/day p.o.) of NPA101.3 for two days and then performing Western blot analysis on protein extracts. As shown in Supplementary Fig. S9, 3 mg/kg/day dose of NPA101.3 strongly inhibited RET

autophosphorylation and signalling as well as VEGFR2 phosphorylation. Then, in order to determine anti-tumorigenic activity and to better distinguish RET- and VEGFR2-mediated effects, we tested NPA101.3 in nude mice transplanted with NIH3T3 cells transformed either by RET/C634Y or HRAS/G12V. Before tumours appeared, animals were treated daily with NPA101.3 (1.0, 3.0 or 10.0 mg/kg/day) or left untreated. NPA101.3 preferentially inhibited RET compared to RAS-driven tumours. While 10.0 mg/kg of compound completely prevented tumour formation induced by oncogenic RET, the treatment reduced, but did not abrogate, formation of tumours driven by RAS; moreover, at lower doses the compound significantly reduced growth of RET-, but not RAS-, driven tumors (Fig. 6). At 1.0 mg/kg, NPA101.3 exhibited strong RET phosphorylation and signalling inhibition in NIH3T3 RET/C634Y tumours (Supplementary information Fig. S10); in contrast, virtually no effect on RAS signalling (MAPK phosphorylation) was detected in NIH3T3 HRAS/G12V tumours. Still, VEGFR2 inhibition was detected also in RAS-driven tumours, an effect that may explain the, albeit reduced, drug effect on their growth (Supplementary information Fig. S11).

DISCUSSION AND CONCLUSIONS

Drug efficacy of a clinical agent is determined by target inhibition and ADMET (adsorption, distribution, metabolism, excretion, and toxicity) profiles (32). During the IND study of the clinical TKI candidate Pz-1, we identified a major, metabolic pathway initiated by Phase 1 demethylation of the Pz-1 methylpyrazole substituent. Here, in order to generate secondary candidates with similar pharmacological profiles to Pz-1 but no propensity to demethylation, we replaced methylpyrazole with the metabolically-resistant bioisostere (methylsulfonyl)benzene. This lead to NPA101.3, a demethylation-resistant clinical candidate optimized for single-agent polypharmacology.

Molecular modelling indicated that, similar to Pz-1, NPA101.3 binds the DFG-out 'inactive' conformation of RET and VEGFR2, thus functioning as a *bona fide* type-2 TKI (31). This is supported experimentally by the relatively large thermal shift observed for the RET kinase-NPA101.3 complex. NPA101.3 exhibited an IC_{50} of 0.001 μM for RET and 0.003 μM for VEGFR2. Noteworthy, similar to Pz-1, NPA101.3 was able to bind tightly to and inhibit (IC_{50} of 0.008 μM) the RET mutant at the gatekeeper site (V804M), which is refractory to the clinical inhibitors Vandetanib and Cabozantinib (31). NPA101.3 featured excellent selectivity for RET and VEGFR2, exhibiting affinity only for few other kinases such as TRKs (TRKA and TRKC), CSF1R, FRK, HCK, LYN and MKNK2. Among them, TRKA and TRKC are well known driver oncogenes, which expands the potential therapeutic application of NPA101.3 beyond RET-driven cancers (43).

In cell-based assays, NPA101.3 inhibited RET autophosphorylation and displayed a potent (IC_{50} between 0.67 and 4.17 nM) growth inhibitory effect on different types of RET (either transfected or endogenously expressing) mutant cells with no detectable effect at doses up to 100 nM in cells negative for RET oncogenes. Finally, NPA101.3 featured efficacy already at 1 mg/kg/day in RET-driven tumours in nude mice. At higher doses (10 mg/kg/day),

NPA101.3 displayed activity also against RAS-driven tumours, likely mediated by VEGFR2 inhibition. Therefore, it is feasible that in a therapeutic setting against RET-driven tumours, activity of the compound may result from a combination of cell autonomous (on tumour cells growth mediated by RET inhibition) and non-cell autonomous (on blood vessels formation mediated by VEGFR2 inhibition) effects.

Several TKIs with anti-RET activity are available and some are already registered for treatment of different types of thyroid cancers. Lesson learned from the use of TKIs in various cancer types has shown that second line inhibitors are clinically useful when first line treatments are hampered by toxicity and/or resistance. Based on potency, selectivity, and balanced RET/VEGFR2 inhibition, we posit that NPA101.3 may represent a promising, demethylation-resistant type-2 TKI for the treatment of RET-driven tumours.

EXPERIMENTAL SECTION

General chemistry procedures and synthesis of NPA101.3. Molecular formula Smiles String:(O=C(NC1=NOC(C(C)(C)C)=C1)CC(C=C2)=CC=C2N(C=N3)C4=C3C=C(C5=CC=C(S(=O)(C)=O)C=C5)C=C4) All solvents were reagent grade or HPLC grade and all starting materials were obtained from commercial sources and used without further purification. Purity of final compounds was assessed using a Shimadzu ultra-high throughput LC/MS system (SIL-20A, LC-20AD, LC-MS 2020, Phenomenex® Onyx Monolithic C-18 Column) at variable wavelengths of 254 nM and 214 nM (Shimadzu PDA Detector, SPD-MN20A) and was >95%, unless otherwise noted. The HPLC mobile phase consisted of a water-acetonitrile gradient buffered with 0.1% formic acid. 1H NMR spectra were recorded at 400 MHz and 13C spectra were recorded at 100 MHz, both completed on a Varian 400 MHz instrument (Model# 4001S41ASP). All compounds were purified using silica gel (0.035-0.070 mm, 60 Å) flash chromatography, unless otherwise noted. Microwave assisted reactions were completed in sealed vessels using a Biotage Initiator microwave synthesizer.

RET kinase assay. Kinase activity was measured by a microfluidic assay that monitors the separation of the phosphorylated product from substrate (31). The assay was run using a 12-sipper chip on a Caliper EZ Reader II (PerkinElmer®, Walthman, USA) with separation buffer (100 mM HEPES, 10 mM EDTA, 0.015% Brij-35, 0.1% CR-3 PerkinElmer®). In 96-well polypropylene plates (Greiner, Frickenhausen, Germany), compound stocks (20 mM in DMSO) were diluted into kinase buffer (50 mM HEPES, 0.075% Brij-35, 0.1 % Tween 20, 2 mM DTT, 10 mM MgCl2, and 0.02% NaN3) in 12-point ½log dilutions (2 mM–6.32 nM). After, 1 μL was transferred into a 384-well polypropylene assay plate (Greiner). The enzymes (Invitrogen™ , Grand Island, USA) were diluted in kinase buffer to a concentration of 2 nM

and 5 μL of the enzyme mixture was transferred to the assay plate. RET, RET/V804M, or VEGFR2 kinases were pre-incubated with the TKI or control buffer, with gentle shaking for 60 min to allow the inhibitor to trap the DFG-out conformation; indeed, it has been reported for the type-2 (DFG-out) p38 inhibitor, BIRB-796, that an increase in incubation time increases activity (44). A substrate mix was prepared containing ATP (Ambresco®, Solon, USA) and substrate peptide dissolved in kinase buffer, and 5 μL of the substrate mix was added to the assay plate. Running concentrations were as follows: ATP (190 μM), peptide (1.5 μM), compound 12-point ½log dilutions (0.2 mM–0.632 nM). For positive control, no inhibitor was added. For negative control, no enzyme was added. The plate was run until 10-20% conversion, based on the positive control wells. The following separation conditions were utilized: upstream voltage -500V; downstream voltage, -1900V; chip pressure -0.8. Percent inhibition was measured for each well comparing starting peptide to phosphorylated product peaks relative to the baseline. Dose response curves, spanning the IC_{50} dose, were generated in GraphPad Prism® 7 and fit to an exponential one-phase decay line; IC_{50} values were obtained from the half-life value of the curve. IC_{50} values were generated in triplicate.

Thermal shift assay. Wild type and V804M mutant RET core kinase domain proteins were expressed in SF21 cells and purified using a GST affinity tag as previously described (45). Subsequently, both proteins were purified and phosphorylated. The affinity tag was removed using HRV 3C protease. To determine the protein thermal shifts, 3μM recombinant proteins were incubated with DMSO (vehicle control), NPA101.3, PP1 or Sorafenib (in 100% DMSO), with a final drug concentration of 40μM, and a final DMSO concentration of 1% (v/v). Sypro-Orange dye (Life Technologies) was added to each drug treatment, and the thermal shift was measured in a QuantStudio 12K Flex Real-Time PCR System (Applied Biosystems) over a

temperature range of 25–90 °C. Subsequent analysis was performed using Protein Thermal Shift Software v1.2 (Applied Biosystems).

Cell cultures. NPA101.3 was dissolved in dimethyl sulfoxide (DMSO) at 50 mM concentration and stored at -80°C. Final dosing solution was prepared on the day of use by dilution of the stock solution in cell growth media. RAT1 cells transformed by the various RET mutants (46) were a kind gift of M. Billaud and were cultured in DMEM with 10% foetal calf serum, 2 mM L-glutamine and 100 units/ml penicillin-streptomycin (GIBCO). NIH3T3 cells transformed by RET/C634Y, HRAS/G12V, CCDC6-RET, NCOA4-RET and FGFR1OP-RET were cultured in DMEM with 5% calf serum, 2 mM L-glutamine and 100 units/mL penicillin-streptomycin (GIBCO). Parental NIH3T3 cells were grown in DMEM with 10% calf serum, 2 mM L-glutamine and 100 units/mL penicillin-streptomycin (GIBCO). All the RET constructs expressed in RAT1 or NIH3T3 cells encoded the short isoform of the RET protein (RET-9). Ba/F3 murine pro-B cells stably expressing NCOA4-RET, RET/C634R and RET/M918T mutant proteins (all cloned in the long RET-51 isoform) were generated by electroporation. Parental and transformed Ba/F3 cells were cultured in RPMI supplemented with 10% foetal calf serum, 2 mM L-glutamine and 100 units/ml penicillin-streptomycin (GIBCO), and, in the case of parental cells, supplemented with 10 ng/ml IL-3. CALU-1, derived from a human lung adenocarcinoma, were grown in EMEM with 10% foetal calf serum, 2 mM L-glutamine and 100 units/mL penicillin-streptomycin (GIBCO). PC-9, derived from a human lung adenocarcinoma, were grown in RPMI with 10% foetal calf serum, 2 mM L-glutamine and 100 units/mL penicillin-streptomycin. Nthy-ori-3-1, derived from normal thyroid follicular tissue and immortalized by SV40 Large T, TPC-1, derived from a human PTC harbouring CCDC6-RET (47), BCPAP, derived from human PTC, 8505-C, derived from a human undifferentiated thyroid cancer, and A549, derived from a human lung

adenocarcinoma, were cultured in DMEM with 10% foetal calf serum, 2 mM L-glutamine and 100 units/mL penicillin-streptomycin. TT, from a human MTC harbouring RET/C634W (48), and MZ-CRC-1, from a human MTC harbouring RET/M918T (a kind gift of R. F. Gagel), were cultured in RPMI with 20% foetal calf serum, 2 mM L-glutamine and 100 units/mL penicillin-streptomycin (GIBCO). Lc-2/ad, derived from human lung adenocarcinoma harbouring CCDC6-RET (49), were grown in RPMI 1640/Ham's F12 (1:1) with 10% foetal calf serum, 2 mM L-glutamine and 100 units/mL penicillin-streptomycin (GIBCO). All the human cell lines were SNP authenticated in 2017.

Immunoblotting. Protein lysates were prepared according to standard procedures. Briefly, cells were lysed in a buffer containing 50 mM N-2-hydroxyethylpiperazine-N'-2-ethanesulfonic acid (HEPES; pH 7.5), 1% (vol/vol) Triton X-100, 150 mM NaCl, 5 mM EGTA, 50 mM NaF, 20 mM sodium pyrophosphate, 1 mM sodium vanadate, 2 mM phenylmethylsulphonyl fluoride (PMSF) and 1 μg/mL aprotinin. Lysates were clarified by centrifugation at 10,000 Xg for 15 min. Lysates containing comparable amounts of proteins, estimated by a modified Bradford assay (Bio-Rad, Munich, Germany), were subjected to direct Western blot. Immune complexes were detected with the enhanced chemiluminescence kit (Amersham Pharmacia Biotech, Little Chalfort, UK). Anti-phospho-SHC (#Y317), that recognizes SHC protein when phosphorylated on Y317, was from Upstate Biotechnology Inc. (Lake Placid, NY). Anti-SHC (H-108) was from Santa Cruz Biotechnology (Santa Cruz, CA). Anti-MAPK (#9101) and anti-phospho-MAPK (#9102), specific for p42/44MAPK (ERK1/2) phosphorylated on Thr202/Tyr204, were from Cell Signalling (Danvers, MA, USA). Anti-phospho-VEGFR2/KDR (#2478), specific for VEGFR2/KDR phosphorylated on Tyr1175 and anti-VEGFR2/KDR (#2479) were from Cell Signalling Technologies (Danvers, MA, USA). Anti-phospho-p70S6K (#9234), specific for p70S6K phosphorylated on Thr389 and

anti-p70S6K (#2708) were from Cell Signalling Technologies (Danvers, MA, USA). Anti-RET is a polyclonal antibody raised against the tyrosine kinase protein fragment of human RET; anti-phospho905 is a phospho-specific polyclonal antibody recognizing RET proteins phosphorylated at Y905 and anti-phospho1062 is a phospho-specific polyclonal antibody recognizing RET proteins phosphorylated at Y1062 (50). Secondary antibodies coupled to horseradish peroxidase were from Santa Cruz Biotechnology.

Cell growth curves. Nthy-ory-3-1 (10,000/well), TPC-1 (10,000/well), MZ-CRC-1 (100,000/well), TT (200,000/well), Lc-2/ad (100,000/well), BCPAP (10,000/well), 8505-C (10,000/well), PC-9 (10,000/well), A549 (10,000/well), CALU-1 (10,000/well), NIH3T3 RET/C634Y (10,000/well) and NIH3T3 HRAS/G12V (10,000/well) were seeded in 6-well tissue culture plates. Cells were kept in 2% (TPC-1), 5% (Nthy-ori-3-1), or 10% (BCPAP, 8505-C, CALU-1, A549, PC-9, TT, MZ-CRC-1 and Lc-2/ad) foetal calf serum or in 2% (NIH3T3 RET/C634Y and HRAS/G12V) calf serum. Ba/F3 cells (200,000/well in 2ml) were seeded in 6-well tissue culture plates and kept in 10% foetal calf serum. The day after plating, different concentrations of drug or vehicle were added to the medium and changed every 2-3 days. Cells were counted every day (Ba/F3), 2 days (fibroblasts) or 2-3 days (human cell lines). To compare cell growth, we performed unpaired Student's *t* test using the Instat software program (Graphpad Software Inc). All *P* values were two-sided, and differences were considered statistically significant at $P < .02$. IC_{50} doses were calculated through a curve fitting analysis from last day of growth curves using the PRISM software program (Graphpad Software Inc).

Mouse xenograft experiments. NPA101.3 was dissolved in 80% H_2O, 19.875% Tween 20, 0.125% Xanthan gum. The formulation was stored at room temperature and vortexed prior to

administration. NIH3T3 RET/C634Y (200,000 cells) or NIH3T3 HRAS/G12V (50,000 cells) were inoculated subcutaneously into dorsal portion (both sides) of 6-week-old female BALB/c nu/nu mice (n. 32 mice/cell line) (Jackson Laboratories, Bar Harbor, Maine). After 4 days, before tumours had appeared, animals were randomly assigned to receive NPA101.3 (1.0, 3.0 or 10 mg/kg daily) (8 mice/group) or vehicle control (8 mice) by oral gavage. Tumour diameters were measured with caliper every 2-3 days. Tumour volumes (V) were calculated by the rotational ellipsoid formula: $V = A \times B^2/2$ (A=axial diameter; B= rotational diameter). No mouse showed signs of wasting or other signs of toxicity. Animals were fed *ad libitum* on an autoclaved diet and tap water and were maintained at the Dipartimento di Medicina Molecolare e Biotecnologie Mediche Animal Facility. All manipulations were performed while the animals were under isoflurane gas anaesthesia. Animal studies were conducted in accordance with Italian regulations for experimentation on animals and approved by the Italian Ministry of health (Authorization n. 1023/2015-PR). To compare tumour growth the unpaired Student's *t* test (InStat program, GraphPad software) was used. *P* values were statistically significant at $P < 0.05$.

ACKNOWLEDGEMENTS

MZ-CRC-1 cells and RAT1 cells expressing RET mutants were kindly donated by R.F. Gagel (MD Anderson Cancer Center, USA) and by M. Billaud (Institut Albert Bonniot, Grenoble, France), respectively.

PDB CODES

VEGFR2 DFG-out crystal structure (PDB# 2OH4)

RET DFG-out model (PDB# 2IVU)

Authors will release the atomic coordinates and experimental data upon article publication.

REFERENCES

REFERENCES

1) Mulligan, L. M. RET revisited: expanding the oncogenic portfolio. *Nat. Rev. Cancer* **2014,** *14*, 173-186.

2) Cancer Genome Atlas Research Network. Integrated genomic characterization of papillary thyroid carcinoma. *Cell* **2014**, *159*, 676-690.

3) Grubbs, E. G.; Ng, P. K.; Bui, J.; Busaidy, N. L.; Chen, K.; Lee, J. E.; Lu, X.; Lu, H.; Meric-Bernstam, F.; Mills, G. B.; Palmer, G.; Perrier, N. D.; Scott, K.L.; Shaw, K. R.; Waguespack, S. G.; Williams, M. D.; Yelensky, R.; Cote, G. J. RET fusion as a novel driver of medullary thyroid carcinoma. *J. Clin. Endocrinol. Metab.* **2015,** *100*, 788-793.

4) Kohno, T.; Ichikawa, H.; Totoki, Y.; Yasuda, K.; Hiramoto, M.; Nammo, T.; Sakamoto, H.; Tsuta, K.; Furuta, K.; Shimada, Y.; Iwakawa, R.; Ogiwara, H.; Oike, T.; Enari, M.; Schetter, A. J.; Okayama, H.; Haugen, A.; Skaug, V.; Chiku, S.; Yamanaka, I.; Arai, Y.; Watanabe, S.; Sekine, I.; Ogawa, S.; Harris, C. C.; Tsuda, H.; Yoshida, T.; Yokota, J.; Shibata, T. KIF5B-RET fusions in lung adenocarcinoma. *Nat. Med.* **2012**, *18*, 375-377.

5) Takeuchi, K.; Soda, M.; Togashi, Y.; Suzuki, R.; Sakata, S.; Hatano, S.; Asaka, R.; Hamanaka, W.; Ninomiya, H.; Uehara, H.; Lim Choi, Y.; Satoh, Y.; Okumura, S.; Nakagawa, K.; Mano, H.; Ishikawa, Y. RET, ROS1 and ALK fusions in lung cancer. *Nat. Med.* **2012**, *18*, 378-381.

6) Lipson, D.; Capelletti, M.; Yelensky, R.; Otto, G.; Parker, A.; Jarosz, M.; Curran, J. A.; Balasubramanian, S.; Bloom, T.; Brennan, K. W.; Donahue, A.; Downing, S. R.; Frampton, G. M.; Garcia, L.; Juhn, F.; Mitchell, K.C.; White, E.; White, J.; Zwirko, Z.; Peretz, T.; Nechushtan, H.; Soussan-Gutman, L.; Kim, J.; Sasaki, H.; Kim, H. R.; Park, S. I.; Ercan, D.; Sheehan, C. E.; Ross, J. S.; Cronin, M. T.; Jänne, P. A.; Stephens, P. J.

Identification of new ALK and RET gene fusions from colorectal and lung cancer biopsies. *Nat Med*. **2012**, *18*, 382-384.

7) Ballerini, P.; Struski, S.; Cresson, C.; Prade, N.; Toujani, S.; Deswarte, C.; Dobbelstein, S.; Petit, A.; Lapillonne, H.; Gautier, E. F.; Demur, C.; Lippert, E.; Pages, P.; Mansat-De Mas, V.; Donadieu, J.; Huguet, F.; Dastugue, N.; Broccardo, C.; Perot, C.; Delabesse, E. RET fusion genes are associated with chronic myelomonocytic leukemia and enhance monocytic differentiation. *Leukemia* **2012**, *26*, 2384-2389.

8) Bossi, D.; Carlomagno, F.; Pallavicini, I.; Pruneri, G.; Trubia, M.; Raviele, P. R.; Marinelli, A.; Anaganti, S.; Cox, M. C.; Viale, G.; Santoro, M.; Di Fiore, P. P.; Minucci, S. Functional characterization of a novel FGFR1OP-RET rearrangement in hematopoietic malignancies. *Mol. Oncol*. **2014**, *8*, 221-231.

9) Wiesner, T.; He, J.; Yelensky, R.; Esteve-Puig, R.; Botton, T.; Yeh, I.; Lipson, D.; Otto, G.; Brennan, K.; Murali, R.; Garrido, M.; Miller, V. A.; Ross, J. S.; Berger, M. F.; Sparatta, A.; Palmedo, G.; Cerroni, L.; Busam, K. J.; Kutzner, H.; Cronin, M. T.; Stephens, P. J.; Bastian, B. C. Kinase fusions are frequent in Spitz tumours and spitzoid melanomas. *Nat. Commun*. **2014**, *5*, 3116.

10) Le Rolle, A. F.; Klempner, S. J.; Garrett, C. R.; Seery, T.; Sanford, E. M.; Balasubramanian, S.; Ross, J. S.; Stephens, P. J.; Miller, V. A.; Ali, S. M.; Chiu, V. K. Identification and characterization of RET fusions in advanced colorectal cancer. *Oncotarget* **2015**, *6*, 28929-28937.

11) Hechtman, J. F.; Zehir, A.; Yaeger, R. D.; Wang, L.; Middha, S.; Zheng, T.; Hyman, D.; Solit, D.; Arcila, M. E.; Borsu, L.; Shia, J.; Vakiani, E.; Saltz, L.; Ladanyi, M. Identification of Targetable Kinase Alterations in Patients with Colorectal Carcinoma that are Preferentially Associated with Wild Type RAS/RAF. *Mol. Cancer Res*. **2016**, *14*, 296-301.

12) Paratala, B. S.; Chung, J. H.; Williams, C. B.; Yilmazel, B.; Petrosky, W.; Williams, K.; Schrock, A. B.; Gay, L. M.; Lee, E.; Dolfi, S. C.; Pham, K.; Lin, S.; Yao, M.; Kulkarni, A.; DiClemente, F.; Liu, C.; Rodriguez-Rodriguez, L.; Ganesan, S.; Ross, J. S.; Ali, S. M.; Leyland-Jones, B.; Hirshfield, K. M. RET rearrangements are actionable alterations in breast cancer. *Nat. Commun.* **2018**, *9*, 4821.

13) Wang, K.; Russell, J. S.; McDermott, J. D.; Elvin, J. A.; Khaira, D.; Johnson, A.; Jennings, T. A.; Ali, S. M.; Murray, M.; Marshall, C.; Oldham, D. S.; Washburn, D.; Wong, S. J.; Chmielecki, J.; Yelensky, R.; Lipson, D.; Miller, V. A.; Stephens, P. J.; Serracino, H. S.; Ross, J. S.; Bowles, D. W. Profiling of 149 Salivary Duct Carcinomas, Carcinoma Ex Pleomorphic Adenomas, and Adenocarcinomas, Not Otherwise Specified Reveals Actionable Genomic Alterations. *Clin. Cancer Res.* **2016**, *22*, 6061-6068.

14) Klempner, S. J.; Bazhenova, L. A.; Braiteh, F. S.; Nikolinakos, P. G.; Gowen, K.; Cervantes, C. M.; Chmielecki, J.; Greenbowe, J. R.; Ross, J. S.; Stephens, P. J.; Miller, V. A.; Ali, S. M.; Ou, S. H. Emergence of RET rearrangement co-existing with activated EGFR mutation in EGFR-mutated NSCLC patients who had progressed on first- or second-generation EGFR TKI. *Lung Cancer* **2015**, *89*, 357-359.

15) Wells, S. A. Jr.; Pacini, F.; Robinson, B. G.; Santoro, M. Multiple endocrine neoplasia type 2 and familial medullary thyroid carcinoma: an update. *J. Clin. Endocrinol. Metab.* **2013**, *98*, 3149-3164.

16) Morandi, A.; Plaza-Menacho, I.; Isacke, C. M. RET in breast cancer: functional and therapeutic implications. *Trends Mol. Med.* **2011**, *17*, 149-157.

17) Nguyen, M.; Miyakawa, S.; Kato, J.; Mori, T.; Arai, T.; Armanini, M.; Gelmon, K.; Yerushalmi, R.; Leung, S.; Gao, D.; Landes, G.; Haak-Frendscho, M.; Elias, K.; Simmons, A. D. Preclinical Efficacy and Safety Assessment of an Antibody-Drug Conjugate

Targeting the c-RET Proto-Oncogene for Breast Carcinoma. *Clin. Cancer Res.* **2015**, *21*, 5552-5562.

18) Gil, Z.; Cavel, O.; Kelly, K.; Brader, P.; Rein, A.; Gao, S. P.; Carlson, D. L.; Shah, J. P.; Fong, Y.; Wong, R. J. Paracrine regulation of pancreatic cancer cell invasion by peripheral nerves. *J. Natl. Cancer Inst.* **2010**, *102*, 107-118.

19) He, S.; Chen, C. H.; Chernichenko, N.; He, S.; Bakst, R. L.; Barajas, F.; Deborde, S.; Allen, P. J.; Vakiani, E.; Yu, Z.; Wong, R. J. GFRα1 released by nerves enhances cancer cell perineural invasion through GDNF-RET signaling. *Proc. Natl. Acad. Sci. U S A* **2014**, *111*, E2008-E2017.

20) De Falco, V.; Carlomagno, F.; Li, HY.; Santoro, M. The molecular basis for RET tyrosine-kinase inhibitors in thyroid cancer. *Best Pract. Res. Clin. Endocrinol. Metab.* **2017**, *31*, 307-318.

21) Drilon, A.; Hu, Z. I.; Lai, G. G. Y. Tan DSW. Targeting RET-driven cancers: lessons from evolving preclinical and clinical landscapes. *Nat. Rev. Clin. Oncol.* **2018**, *15*, 151-167.

22) Commander, H.; Whiteside, G.; Perry, C. Vandetanib: first global approval. Drugs **2011**, *71*, 1355-1365.

23) Grüllich, C. Cabozantinib: a MET, RET, and VEGFR2 tyrosine kinase inhibitor. *Recent Results Cancer Res.* **2014**, *201*, 207-214.

24) Wells, S. A. Jr.; Robinson, B. G.; Gagel, R. F.; Dralle, H.; Fagin, J. A.; Santoro, M.; Baudin, E.; Elisei, R.; Jarzab, B.; Vasselli, J. R.; Read, J.; Langmuir, P.; Ryan, A. J.; Schlumberger, M. J. Vandetanib in patients with locally advanced or metastatic medullary thyroid cancer: a randomized, double-blind phase III trial. *J. Clin. Oncol.* **2012**, *30*, 134-141.

25) Elisei, R.; Schlumberger, M. J.; Müller, S. P.; Schöffski, P.; Brose, M. S.; Shah, M. H.; Licitra, L.; Jarzab, B.; Medvedev, V.; Kreissl, M. C.; Niederle, B.; Cohen, E. E.; Wirth, L.

J.; Ali, H.; Hessel, C.; Yaron, Y.; Ball, D.; Nelkin, B.; Sherman, S. I. Cabozantinib in progressive medullary thyroid cancer. *J. Clin. Oncol.* **2013**, *31*, 3639-3646.

26) Schlumberger, M.; Tahara, M.; Wirth, L. J.; Robinson, B.; Brose, M. S.; Elisei, R.; Habra, M. A.; Newbold, K.; Shah, M. H.; Hoff, A. O.; Gianoukakis, A. G.; Kiyota, N.; Taylor, M. H.; Kim, S. B.; Krzyzanowska, M. K.; Dutcus, C. E.; de las Heras, B.; Zhu, J.; Sherman, S. I. Lenvatinib versus placebo in radioiodine-refractory thyroid cancer. *N. Engl. J. Med.* **2015**, *372*, 621-630.

27) White, P. T.; Cohen, M. S. The discovery and development of sorafenib for the treatment of thyroid cancer. *Expert Opin. Drug Discov.* **2015**, *10*, 427-439.

28) Subbiah, V.; Gainor, J. F.; Rahal, R.; Brubaker, J. D.; Kim, J. L.; Maynard, M.; Hu, W.; Cao, Q.; Sheets, M. P.; Wilson, D.; Wilson, K. J.; DiPietro, L.; Fleming, P.; Palmer, M.; Hu, M. I.; Wirth, L.; Brose, M. S.; Ou, S. I.; Taylor, M.; Garralda, E.; Miller, S.; Wolf, B.; Lengauer, C.; Guzi, T.; Evans, E. K. Precision Targeted Therapy with BLU-667 for RET-Driven Cancers. *Cancer Discov.* **2018**, *8*, 836-849.

29) Subbiah, V.; Velcheti, V.; Tuch, B. B.; Ebata, K.; Busaidy, N. L.; Cabanillas, M. E.; Wirth, L. J.; Stock, S.; Smith, S.; Lauriault, V.; Corsi-Travali, S.; Henry, D.; Burkard, M.; Hamor, R.; Bouhana, K.; Winski, S.; Wallace, R. D.; Hartley, D.; Rhodes, S.; Reddy, M.; Brandhuber, B. J.; Andrews, S.; Rothenberg, S. M.; Drilon, A. Selective RET Kinase Inhibition for Patients with RET-Altered Cancers. *Ann. Oncol.* **2018**; *29*, 1869-1876.

30) Drilon, A.; Fu, S.; Patel, M. R.; Fakih, M.; Wang, D.; Olszanski, A. J.; Morgensztern, D.; Liu, S. V.; Cho, B. C.; Bazhenova, L.; Rodriguez, C. P.; Doebele, R. C.; Wozniak, A.; Reckamp, K. L.; Seery, T.; Nikolinakos, P.; Hu, Z.; Oliver, J. W.; Trone, D.; McArthur, K.; Patel, R.; Multani, P. S.; Ahn, M. J. A Phase I/Ib Trial of the VEGFR-Sparing Multikinase RET Inhibitor RXDX-105. *Cancer Discov.* **2019**, *9*, 384-395.

31) Frett, B.; Carlomagno, F.; Moccia, M. L.; Brescia, A.; Federico, G.; De Falco, V.; Admire, B.; Chen, Z.; Qi, W.; Santoro, M.; Li, HY. Fragment-Based Discovery of a Dual pan-RET/VEGFR2 Kinase Inhibitor Optimized for Single-Agent Polypharmacology. *Angew. Chem. Int. Ed. Engl.* **2015**, *54*, 8717-8721.

32) Yamazaki, H. Drug-Metabolizing Enzyme Systems I. In *Comprehensive Medicinal Chemistry III*; Chackalamannil, S.; Rotella, D.; Ward, S. Eds: Elsevier, 2017; pp 45-50.

33) Zhang, J.; Yang, P. L.; Gray, N. S. Targeting cancer with small molecule kinase inhibitors. *Nat. Rev. Cancer* **2009**, *9*, 28-39.

34) Carlomagno, F.; Guida, T.; Anaganti, S.; Vecchio, G.; Fusco, A.; Ryan, A. J.; Billaud, M.; Santoro, M. Disease associated mutations at valine 804 in the RET receptor tyrosine kinase confer resistance to selective kinase inhibitors. *Oncogene* **2004**, *23*, 6056-6063.

35) Mologni, L.; Redaelli, S.; Morandi, A.; Plaza-Menacho, I.; Gambacorti-Passerini, C. Ponatinib is a potent inhibitor of wild-type and drug-resistant gatekeeper mutant RET kinase. *Mol. Cell. Endocrinol.* **2013**, *377*, 1-6.

36) Plenker, D.; Riedel, M.; Brägelmann, J.; Dammert, M. A.; Chauhan, R.; Knowles, P. P.; Lorenz, C.; Keul, M.; Bührmann, M.; Pagel, O.; Tischler, V.; Scheel, A. H.; Schütte, D.; Song, Y.; Stark, J.; Mrugalla, F.; Alber, Y.; Richters, A.; Engel, J.; Leenders, F.; Heuckmann, J. M.; Wolf, J.; Diebold, J.; Pall, G.; Peifer, M.; Aerts, M.; Gevaert, K.; Zahedi, R. P.; Buettner, R.; Shokat, K. M.; McDonald, N. Q.; Kast, S. M.; Gautschi, O.; Thomas, R. K.; Sos, M. L. Drugging the catalytically inactive state of RET kinase in RET-rearranged tumors. *Sci. Transl. Med.* **2017**, *9*, 394.

37) Vedadi, M.; Niesen, F. H.; Allali-Hassani, A.; Fedorov, O. Y.; Finerty, P. J. Jr.; Wasney, G. A.; Yeung, R.; Arrowsmith, C.; Ball, L. J.; Berglund, H.; Hui, R.; Marsden, B. D.; Nordlund, P.; Sundstrom, M.; Weigelt, J.; Edwards, A. M. Chemical screening methods

to identify ligands that promote protein stability, protein crystallization, and structure determination. *Proc. Natl. Acad. Sci. U S A* **2006**, *103*, 15835-15840.

38) Nakaoku, T.; Kohno, T.; Araki, M.; Niho, S.; Chauhan, R.; Knowles, P. P.; Tsuchihara, K.; Matsumoto, S.; Shimada, Y.; Mimaki, S.; Ishii, G.; Ichikawa, H.; Nagatoishi, S.; Tsumoto, K.; Okuno, Y.; Yoh, K.; McDonald, N. Q.; Goto, K. A secondary RET mutation in the activation loop conferring resistance to vandetanib. *Nat. Commun.* **2018**, *9*, 625.

39) Bullock, A. N.; Debreczeni, J. E.; Fedorov, O. Y.; Nelson, A.; Marsden, B. D.; Knapp, S. Structural basis of inhibitor specificity of the human protooncogene proviral insertion site in moloney murine leukemia virus (PIM-1) kinase. *J. Med. Chem.* **2005**, *48*, 7604-7614.

40) Kufareva, I.; Abagyan, R. Type-II kinase inhibitor docking, screening, and profiling using modified structures of active kinase states. *J. Med. Chem.* **2008**, *51*, 7921-7932.

41) Plaza-Menacho, I.; Barnouin, K.; Goodman, K.; Martínez-Torres, R. J.; Borg, A.; Murray-Rust, J.; Mouilleron, S.; Knowles, P.; McDonald, N. Q. Oncogenic RET kinase domain mutations perturb the autophosphorylation trajectory by enhancing substrate presentation in trans. *Mol. Cell* **2014**, *53*, 738-751.

42) Kitayama, H.; Kanakura, Y.; Furitsu, T.; Tsujimura, T.; Oritani, K.; Ikeda, H.; Sugahara, H.; Mitsui, H.; Kanayama, Y.; Kitamura, Y. Constitutively activating mutations of c-kit receptor tyrosine kinase confer factor-independent growth and tumorigenicity of factor-dependent hematopoietic cell lines. *Blood* **1995**, *85*, 790-798.

43) Yan, W.; Lakkaniga, N. R.; Carlomagno, F.; Santoro, M.; McDonald, N. Q.; Lv, F.; Gunaganti, N.; Frett, B.; Li, HY. Insights into Current Tropomyosin Receptor Kinase (TRK) Inhibitors: Development and Clinical Application. *J. Med. Chem.* **2019**, *62*, 1731-1760.

44) Pargellis, C.; Tong, L.; Churchill, L.; Cirillo, P. F.; Gilmore, T.; Graham, A. G.; Grob, P. M.; Hickey, E. R.; Moss, N.; Pav, S.; Regan, J. Inhibition of p38 MAP kinase by utilizing a novel allosteric binding site. *Nat. Struct. Biol.* **2002**, *9*, 268-272.

45) Knowles, P. P.; Murray-Rust, J.; Kjaer, S.; Scott, R. P.; Hanrahan, S.; Santoro, M.; Ibáñez, C. F.; McDonald, N. Q. Structure and chemical inhibition of the RET tyrosine kinase domain. *J. Biol. Chem.* **2006**, *281*, 33577-33587.

46) Pasini, A.; Geneste, O.; Legrand, P.; Schlumberger, M.; Rossel, M.; Fournier, L.; Rudkin, B. B.; Schuffenecker, I.; Lenoir, G. M.; Billaud, M. Oncogenic activation of RET by two distinct FMTC mutations affecting the tyrosine kinase domain. *Oncogene* **1997**, *15*, 393-402.

47) Ishizaka, Y.; Ushijima, T.; Sugimura, T.; Nagao, M. cDNA cloning and characterization of ret activated in a human papillary thyroid carcinoma cell line. *Biochem. Biophys. Res. Commun.* **1990**, *168*, 402-408.

48) Carlomagno, F.; Salvatore, D.; Santoro, M.; de Franciscis, V.; Quadro, L.; Panariello, L.; Colantuoni, V.; Fusco, A. Point mutation of the RET proto-oncogene in the TT human medullary thyroid carcinoma cell line. *Biochem. Biophys. Res. Commun.* **1995**, *207*, 1022–1028.

49) Suzuki, M.; Makinoshima, H.; Matsumoto, S.; Suzuki, A.; Mimaki, S.; Matsushima, K.; Yoh, K.; Goto, K.; Suzuki, Y.; Ishii, G.; Ochiai, A.; Tsuta, K.; Shibata, T.; Kohno T, Esumi, H.; Tsuchihara, K. Identification of a lung adenocarcinoma cell line with CCDC6-RET fusion gene and the effect of RET inhibitors in vitro and in vivo. *Cancer Sci.* **2013**, *104*, 896-903.

50) Carlomagno, F.; Vitagliano, D.; Guida, T.; Basolo, F.; Castellone, M. D.; Melillo, R. M.; Fusco, A.; Santoro, M. Efficient inhibition of RET/papillary thyroid carcinoma oncogenic

kinases by 4-amino-5-(4-chloro-phenyl)-7-(t-butyl)pyrazolo[3,4-d]pyrimidine (PP2). *J. Clin. Endocrinol. Metab.* **2003**, *88*, 1897-1902.

FIGURES and LEGENDS

Fig. 1

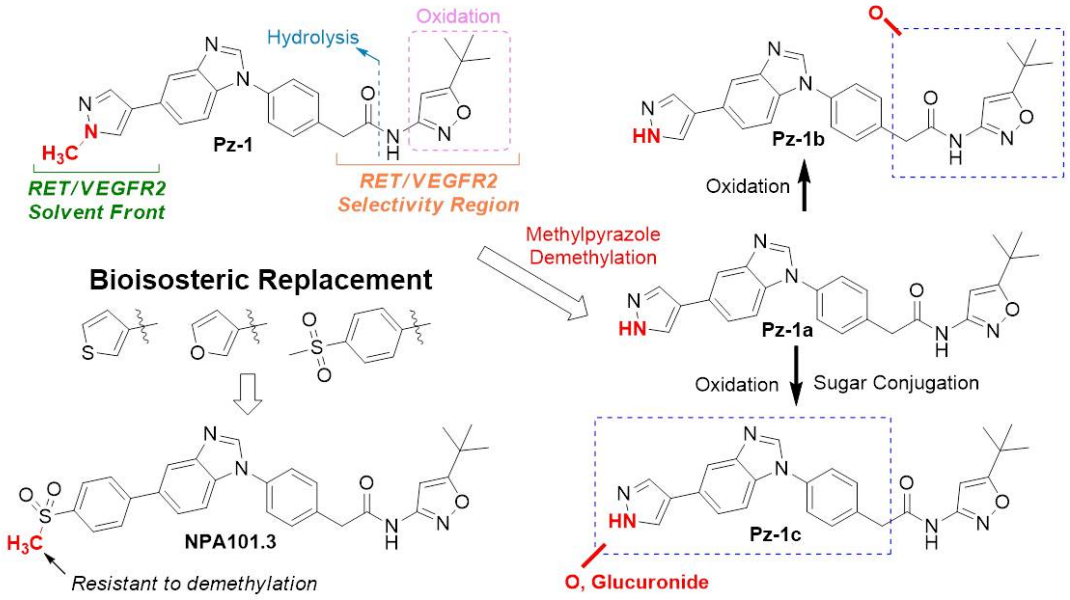

Figure 1: Metabolism of Pz-1 and Bioisosteric Replacement Methods — Pz-1 is hydrolyzed, oxidized, or demethylated via Phase 1 metabolic systems. Hydrolysis and oxidation occur in the selectivity region for binding to RET and VEGFR2, while demethylation occurs at the solvent front for both kinases. Bioisosteric replacement at the solvent front was performed by replacing methylpyrazole with (methylsulfonyl)benzene, generating NPA101.3. VEGFR2 DFG-out crystal structure (PDB# 2OH4); RET DFG-out model (PDB# 2IVU)

Fig. 2

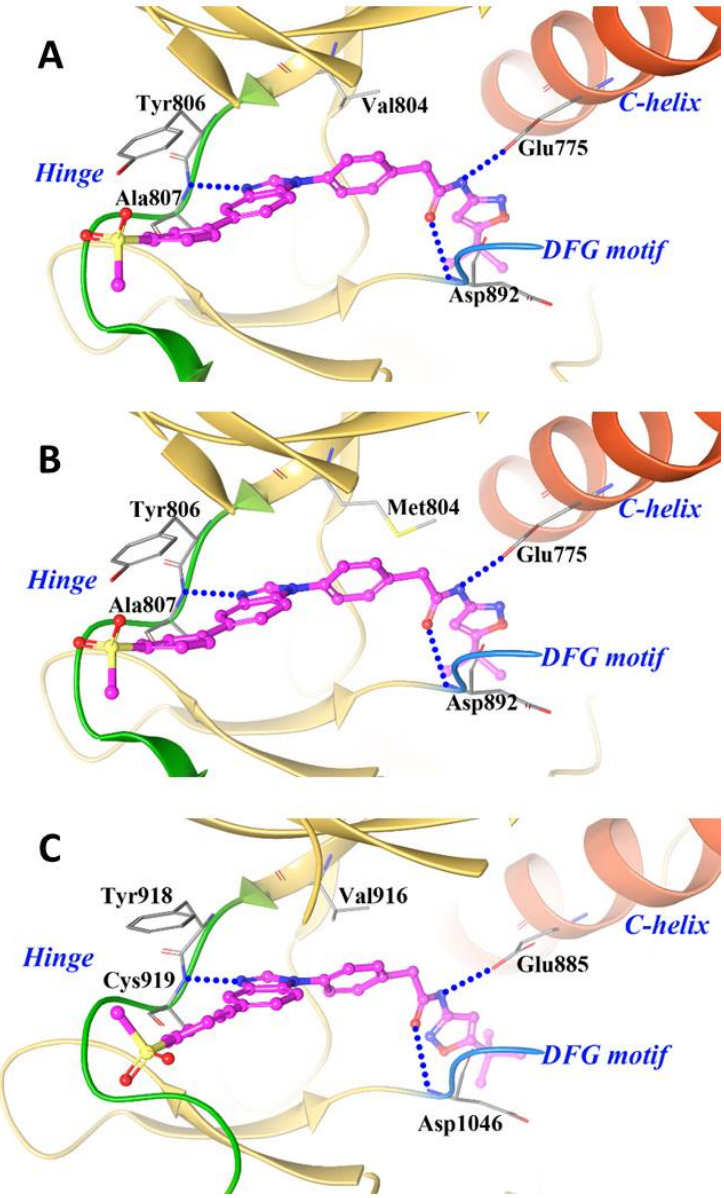

Figure 2: Computational modelling of NPA101.3 — (A) NPA101.3 computationally modelled in a RET DFG-out homology model. The model shows the hydrogen bond at the ATP binding site with A807, a hydrogen bond network at the DFG motif, and interaction with Y806 via π-π stacking. The model also shows that *p*-sulfone of NPA101.3 is solvent exposed. Hydrogen bonds are shown with blue dotted lines. (B) NPA101.3 computationally modelled in a RET/V804M DFG-out homology model. NPA101.3 is able to accommodate bulky mutations at the gatekeeper residue. (C) NPA101.3 computationally modelled in the VEGFR2 kinase. The binding mode is near identical to the binding in RET, with exception of the isoxazole orientation in the allosteric pocket. Flexibility at the methylene linker is predicted to permit the balanced affinity of NPA101.3 to RET and VEGFR2.

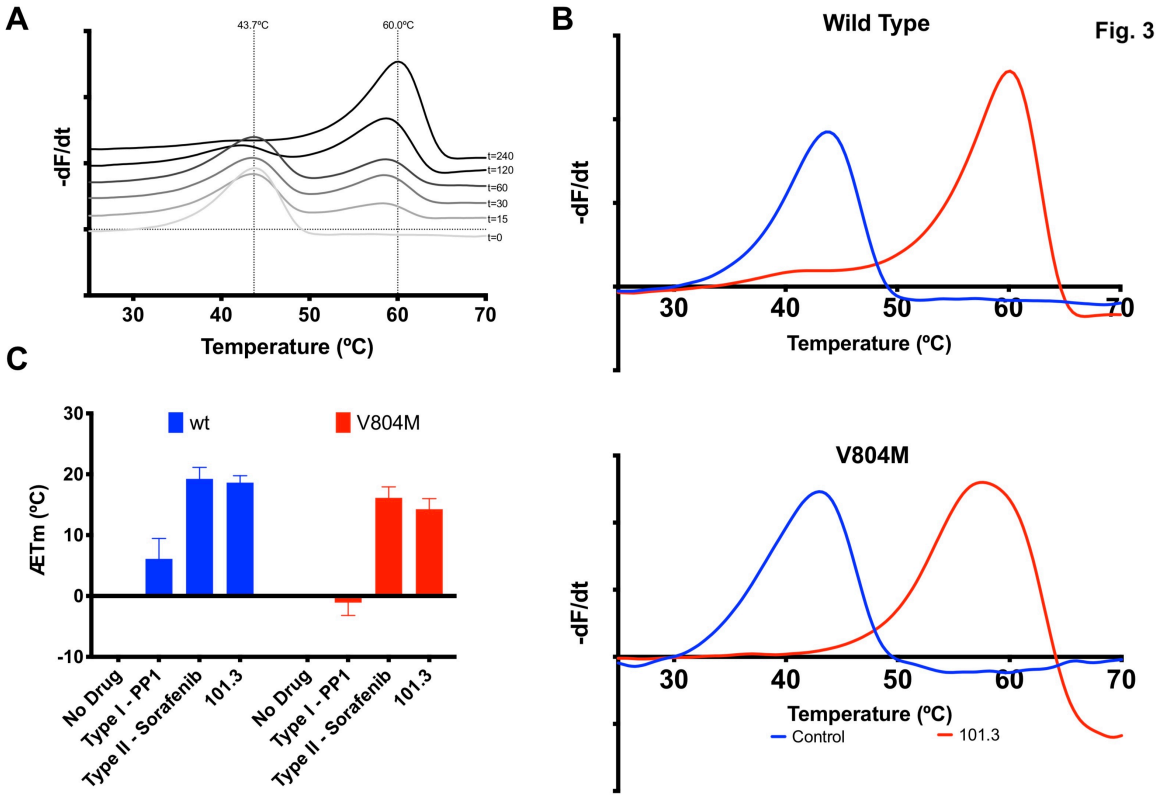

Fig. 3

Figure 3: Thermal shift assay determination of the type-2 binding mode of NPA101.3 — (A) Representative experiment of binding of NPA101.3 to wild type RET core kinase domain monitored by the change in thermal stability. The melting temperature Tm is obtained from the first derivative of the change in fluorescence (-dF/dt) taken from the top of the peak in the derivative plot. (B) Plot of the derivative of the change in fluorescence (-dF/dt) for the wild type protein or V804M mutant in the presence of NPA101.3 or buffer for a representative experiment. The compound binds equally well to either RET protein (C) Tabulated average melting temperature differences (ΔTm) from four independent experiments after addition of NPA101.3, PP1 (a known type-1 inhibitor) or Sorafenib (a known type-2 inhibitor). The respective SD errors are shown for each drug.

Fig. 4

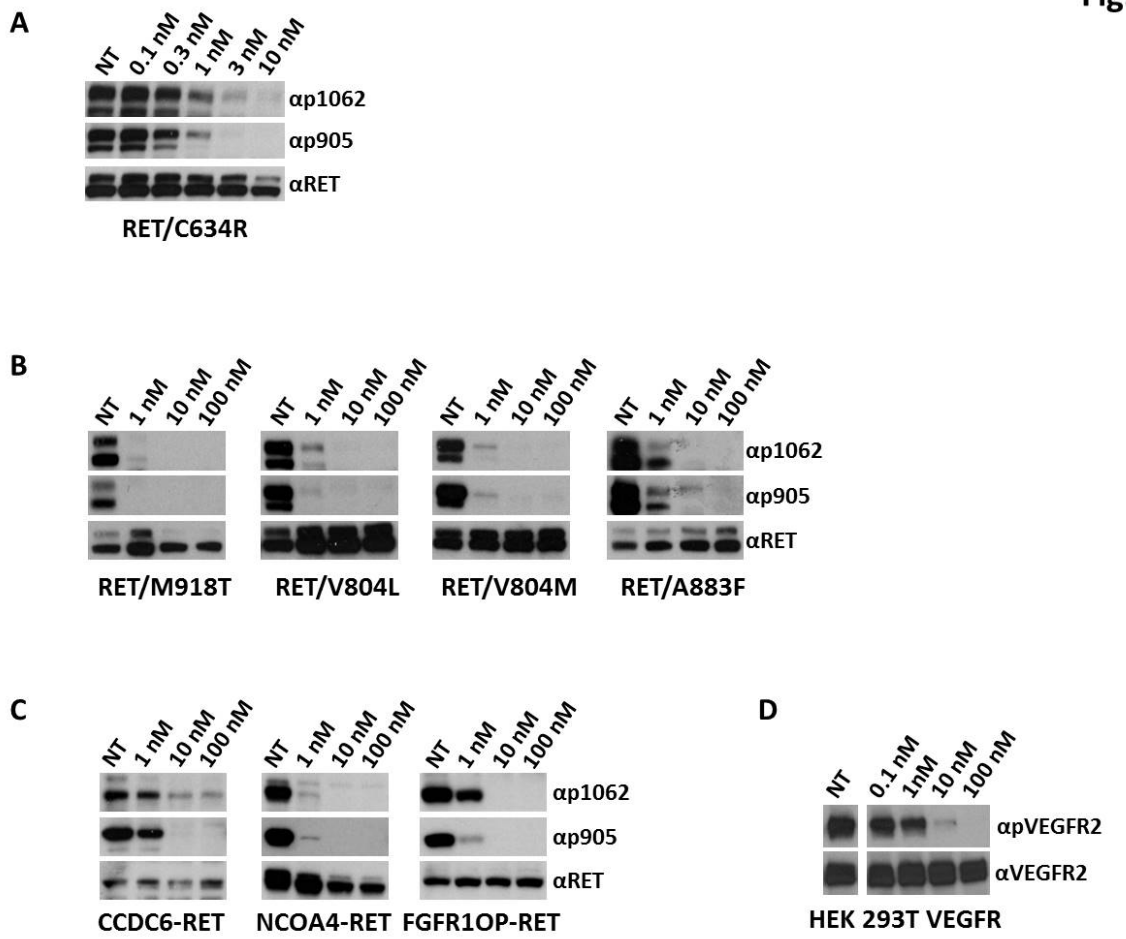

Figure 4: NPA101.3-mediated inhibition of phosphorylation and signalling of oncogenic RET mutants and VEGFR2 in intact cells — Serum-starved RAT1 cells exogenously expressing the indicated RET point mutants (A, B) or NIH3T3 cells exogenously expressing the indicated RET rearranged mutants (C) were treated for 2 hr with indicated concentrations of compound. Total cell lysates (50 μg) were subjected to immunoblotting with anti-phospho-Y1062 (αp1062) and anti-phospho-Y905 (αp905) RET antibodies. The blots were normalized using anti-RET (αRET) antibody. D) HEK293 cells were transiently transfected with human VEGFR2; 36 hr after transfection, cells were serum starved for 12 hr. The indicated doses of compound or vehicle (NT) were added for 2 hr and then VEGFA (100 ng/ml) stimulation was applied for 15 min. Cell lysates were immunoblotted with anti-phospho-VEGFR2 (αpVEGFR2) antibody. The blot was normalized using anti-VEGFR2 (αVEGFR2) antibody.

Fig. 5

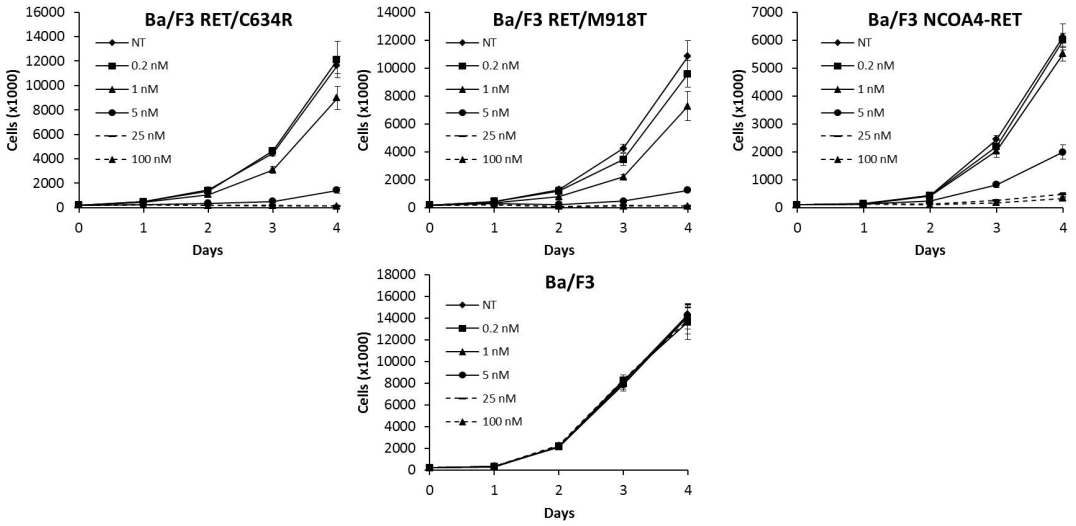

IC_{50} dose

Ba/F3 RET/C634R	1.7 nM (1.4-2.2 nM)
Ba/F3 RET/M918T	1.6 nM (1.2-2.1 nM)
Ba/F3 NCOA4-RET	3.1 nM (2.6-3.6 nM)
Ba/F3	>100 nM

Figure 5: NPA101.3-mediated inhibition of proliferation of RET-transformed Ba/F3 cells — Parental and RET/C634R, RET M918T and NCOA4-RET transfected Ba/F3 cells were incubated with vehicle (NT: not treated) or the indicated concentrations of NPA101.3 and counted at the indicated time points. Parental cells were supplemented with IL3 (10 ng/ml). Data are the mean ± SD of a single experiment performed in triplicate. Growth inhibition IC_{50} doses of the compound for the different cell lines are reported. 95% CI are indicated in brackets.

Fig. 6

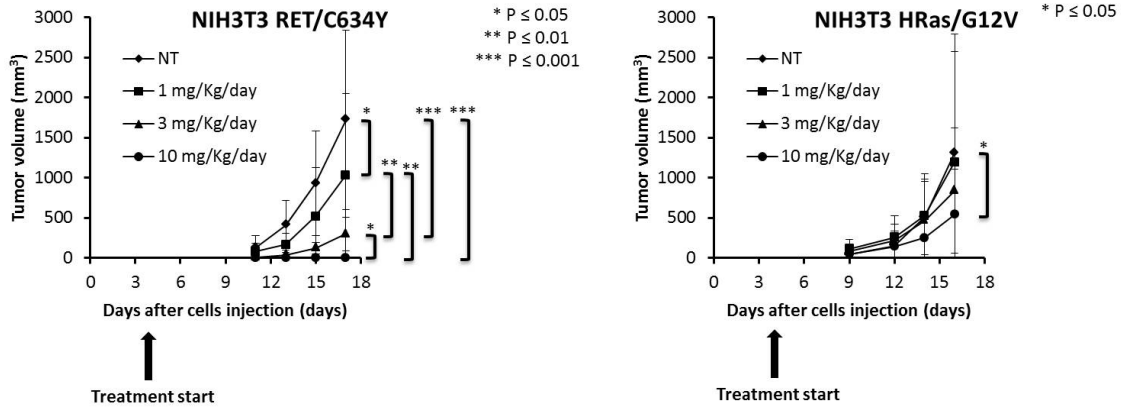

Figure 6: Effects of NPA101.3 on *in vivo* tumour growth — NIH3T3 cells transformed by RET/C634Y or HRAS/G12V were inoculated subcutaneously into nu/nu mice. After 4 days, animals were randomly assigned to receive for the indicated time periods the compound (1.0, 3.0 or 10 mg/kg daily) (24 mice: 8 mice/group for 1, 3 and 10 mg/kg doses) or vehicle (8 mice) by oral gavage. Average size of tumors is reported ± SD.

Table of Contents graphic

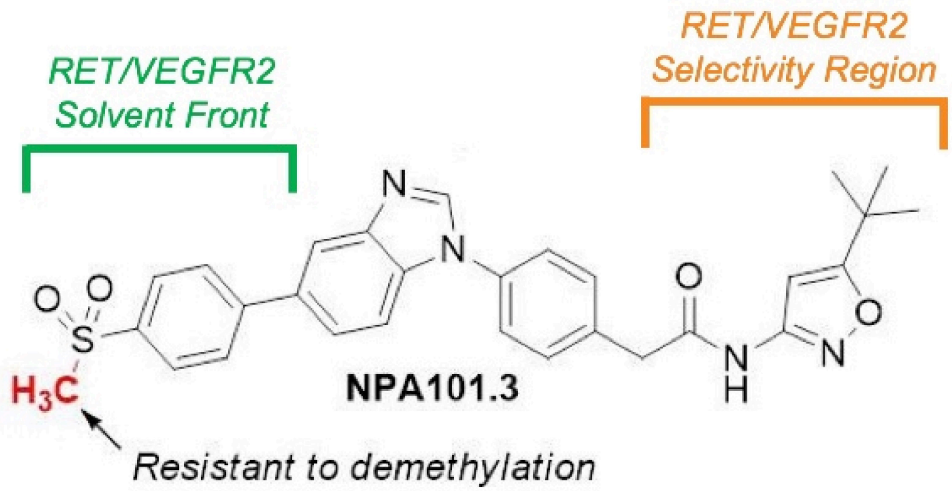

VEGFR2 IC_{50}	3 nM
RET $IC_{50.}$	1 nM